RSC Advances

ROYAL SOCIETY OF CHEMISTRY

www.rsc.org/advances

Bismuth-based nanoparticles as the environmentally – friendly replacement for lead-based piezoelectrics

Margarita Esquivel-Gaon[a], Sergio Anguissola[b] David Garry[b] Adriana del C. Gallegos Melgar[c] Juan Muñoz Saldaña[c], Kenneth A. Dawson[b], Andrea De Vizcaya-Ruiz[a*], Luz M. Del Razo[a*].

Abstract

The use of nanotechnology in the piezoelectric industry conveys new concerns about the environmental toxicity related to lead based nanomaterials. Perovskite structured materials are extensively used as piezoelectrics, lead zirconate titanate (PZT) being the primary choice for sensors, actuators, etc., because of its powerful electromechanical conversion. However, during the life cycle of PZT piezoelectrics lead generally leaches into the environment over time, leading to human exposure and potential environmental hazard. Lead-free bismuth based- ferroelectric materials (BNT-BT) are promising substitutes due to their ability to provide all the piezoelectric attributes without leaching toxic material. Yet, little is known about the potential toxicity and interactions of these nanomaterials with biomolecules and their subsequent intracellular localization at the nanoscale. The aim of this study was to compare the biological impact and uptake of lead and bismuth-based piezoelectric nanoparticles in order to present a suitable substitute for the piezoelectric industry. Our results show that BNT-BT and PZT nanoparticles were internalized through the endolysosomal pathway following a first order kinetic, nanoparticles were localized in the lamellar bodies without inducing cell toxicity measured by mitochondrial activity and cell membrane integrity. Furthermore, BNT-BT nanoparticles were more stable as lead-based PZT released 20% more lead ions into cell culture media. Finally, we propose bismuth-based BNT-BT as a suitable candidate for commercial use as they avoid environmental leaching, imposing less risk during manufacturing and in occupational health, beside the high biocompatibility and similar physico-chemical properties.

Introduction

Engineered nanoparticles show unique characteristics between 1 and 100 nm such as enhanced surface area, electronic, optical, and magnetic properties when compared to the same material in bulk size.[1, 2] Advancements in ferroelectric properties of these materials at the nanoscale has increased the use of nanotechnology in the piezoelectric industry and with that has generated concerns related to the toxicity of these materials. Piezoelectric materials are used in a multitude of devices such as sensors, actuators, multilayered capacitors, and transducers, these applications include nanoelectronics, fuel cells and energy storage[3] amongst others with a wide market worldwide.[4, 5] Due to its strong electromechanical properties lead zirconate titanate or PZT is one of the most widely used piezoelectric materials,[4, 6] however, the main concern is the constant presence of lead-oxide in its structure as this molecule becomes volatile during the manufacturing process or waste disposal. The leaching of lead oxide from devices results in environmental pollution and thus imposing a potential occupational or environmental risk from its exposure,[7] with probable irreversible alterations to the immune, renal, hepatic, and reproductive systems.[8] Initiatives such as RoHs (Restriction of Hazardous Substances) and WEEE (Waste Electrical and Electronic Equipment) restrict the use of hazardous metals such as lead and these initiatives have been adopted by several European countries in the last decade. However, many products with piezoelectric characteristics such as electronic devices still use lead as a key element in their composition.[4, 9] A shift to the use of lead-free nanomaterials is only sustainable if a non-toxic alternative is established. One of the promising candidates to replace lead-based nanomaterials is the pseudobinary system formed by bismuth, sodium, barium, and titanium ((0.94) $Bi_{0.5}$ $Na_{0.5}$ TiO_3 – 0.06 $BaTiO_3$) known as BNT-BT.[10] BNT-BT is a perovskite structured piezoelectric material with properties such as a high remanent polarization, electrochemical, and pyroelectric characteristics at the morphotropic phase boundary (MPB) composition, which makes this system suitable to replace the lead-based PZT.[5, 7, 9] Moreover, bismuth, the primary component in BNT-BT, is a non-toxic metal used especially in the pharmaceutical industry.[11, 12] However, little is known

about the potential toxic behavior of these materials at the nanoscale which makes a risk assessment study a necessity in order to find a replacement for PZT.

Human exposure to nanoparticles occurs during every step of their life cycle; the principal portal of entry of nanoparticles during human exposure is the respiratory system through inhalation.[13-15] Nanoparticles that reach the alveolar region can interact with pneumocytes, leading to nanoparticle uptake with potential toxic downstream effects.[2] The internalization of nanoparticles in non-phagocytic cells is carried out by endocytic mechanisms including macropinocytosis, caveolin or clathrin dependent pathways, or lipid raft-dependent mechanisms.[16, 17] Endocytosis of nanoparticles dispersed in biological fluids is regulated by a bio-nano interface defined as the biomolecular corona.[16] This dynamic process of adsorption/desorption of biomolecules allows nanoparticle to access the cell by endocytic mechanisms and controls subcellular localization and potential biological outcomes. Several mechanisms of toxicity have been identified following exposure of nanoparticles to cells, including generation of reactive oxygen species, disruption of lysosomal functionality, induction of apoptotic and necrotic cells death or genotoxicity.[18] Another important factor responsible for toxicity of nanoparticles is the dissolution of metallic ions from the surface of nanoparticles in the cellular environment thus, compromising cellular homeostasis due to the induction of oxidative stress.[19] Due to the plethora of possible biological endpoints based on the variety of nanoparticles and their physico-chemical characteristics, a thorough biosafety assessment of each new nanomaterial should be performed before the above mentioned devices, which contain them, are released into the market. In this study, we compare the dissolution of BNT-BT and PZT nanoparticles and the toxic effects and uptake of the two piezoelectric materials in the nanoscale in order to demonstrate the suitability of BNT-BT as a substitute for lead based nanoparticles in future technologies. In this paper, we present information about the physicochemical characterization of BNT-BT and PZT, as well as data about the cellular toxicity such as cell count, nuclear morphology, cell membrane integrity, mitochondrial membrane potential, and lysosomal physiology in the same experimental design to provide a holistic approach to nanoparticle toxicity assessment. Additionally, qualitative and quantitative analysis of BNT-BT and PZT nanoparticles was assessed by

atomic spectrometry in a pulmonary cell line. We further demonstrate that both BNT-BT and PZT nanoparticles were internalized through the endolysosomal pathway without high dissociation of the nanoparticle components and therefore no toxic effects.

Results and discussion

Nanoparticle characterization

Finding a replacement for lead (due to its toxic effects during the manufacturing process) in piezoelectrics applications has been an issue for many years; Further, little is known about the potential adverse properties of these and many other materials in the nanoscale introduced in industrial, medical and consumer products. Thus, there is a need to assess the risk of PZT nanoparticles and their replacement candidate BNT-BT nanoparticles.

First it was necessary to assess the physicochemical characteristics as the size distribution of the nanoparticle dispersions. Dynamic Light Scattering (DLS) measurement reported a diameter in saline solution of 194.6 ± 1.0 nm for BNT-BT and 167 ± 1.7 nm for PZT nanoparticles (Figure 1a and Figure S1). The Polydispersity Index (PDI) was less than 0.15 for both nanoparticle dispersions, indicating an adequate degree of monodispersity (Figure 1a). Differential Centrifugal Sedimentation (DCS) measurements showed curves that were similar to the ones obtained by DLS (Figure 1a and Figure S1).

Nanoparticle average size diameter in cell culture media showed an increase of approximately 30 nm probably due to the aggregation of nanoparticles (Figure S1). Furthermore, the results suggested that both dispersions had comparable size and surface charge. Additionally, representative SEM (Figure 1b) and TEM (Figure 1c) images of BNT-BT and PZT nanoparticles showed a range of sizes between 60 and 200 nm, with a majority under 100 nm, which was consistent with DLS and DCS data.

a

	DCS peak (nm)	Z-average (nm)	PDI	ζ Potential (mV)
BNT BT	189	194.6 ± 1.0	0.138 ± 0.025	- 14.9 ± 0.66
PZT	161	167 ± 1.7	0.128 ±0.018	-15.7 ±1.65

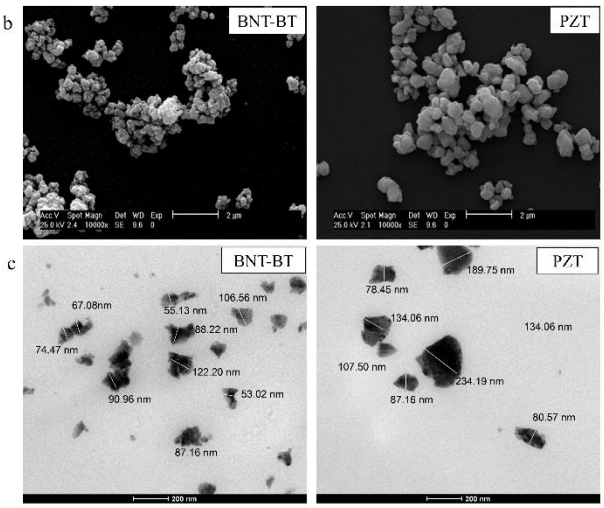

Figure 1. Physicochemical characterization of BNT-BT and PZT nanoparticles. The samples in powder form were dispersed using phosphate buffer and BSA, as described in Materials and Methods. The zeta potential was assessed by Laser Doppler Electrophoresis (a). The size of both nanoparticles was assessed by DLS and DCS (a), SEM (b), TEM (c).

Presence of bismuth or lead in the nanoparticle and ions leaching into cell culture media

Bismuth and lead content for total nanoparticle concentration and dissolved ion concentration were tested for BNT-BT and PZT as described in the Experimental section. Atomic spectrometry indicated that bismuth content in BNT-BT nanoparticles was 37%, while the percentage of lead in PZT nanoparticles was 50%. Additionally, the leaching of PZT detected in the biological media was up to ten times higher when compared with BNT-BT. This indicates that far higher quantities of lead ions are being released in the surrounding environment leading to unwanted side effects to neighbouring cells[20]. Table 1 shows the concentration (µg/ml) of bismuth and lead that correspond to the nominal concentration of nanoparticles in cell culture medium.

Table 1. Comparison between bismuth and lead concentration in cell culture medium and supernatant* evaluated by atomic spectrometry.**

	Nanoparticle nominal concentration (µg/ml)	Bismuth (µg/ml) in BNT-BT nanoparticles	Lead (µg/ml) in PZT Nanoparticles
In DMEM	12.5	5.51 ± 0.01	7.19 ± 0.61
	25	10.23 ± 0.45	12.51 ± 1.17
	50	19.45 ± 3.36	23.73 ± 2.3
In Supernatant	12.5	0.05 ± 0.004	0.52 ± 0.01
	25	0.11 ± 0.04	0.82 ± 0.04
	50	0.42 ± 0.01	1.16 ± 0.05

* The supernatant fraction was obtained after the centrifugation of 1ml of nanoparticles in cDMEM at 20000 g for 1h.

** Bismuth content was detected by atomic fluorescence spectrometry while lead content was detected by atomic absorption spectrometry

BNT-BT and PZT nanoparticle exposure does not exert cytotoxic effects on A549 cells

Taking into account that the respiratory system is an important portal of entry for any contaminants including nanoparticles. We selected human alveolar A549 cells to evaluate the pulmonary response given after the exposure to BNT-BT and PZT nanoparticles. In order to approximate a risk assessment we employed High Content Analysis (HCA) which is an established in vitro screening approach in drug discovery and toxicology[21] and is rapidly becoming a leading platform for risk assessment of nanomaterials.[18] The parameters employed by HCA to analyse cytotoxicity of BNT-BT and PZT nanoparticles were cell number and nuclear morphology, nuclear size and intensity, alteration in lysosomal pH, mitochondrial membrane potential and integrity of the plasma membrane,[18] representative images are shown in Figure 2 and Figure S2b.

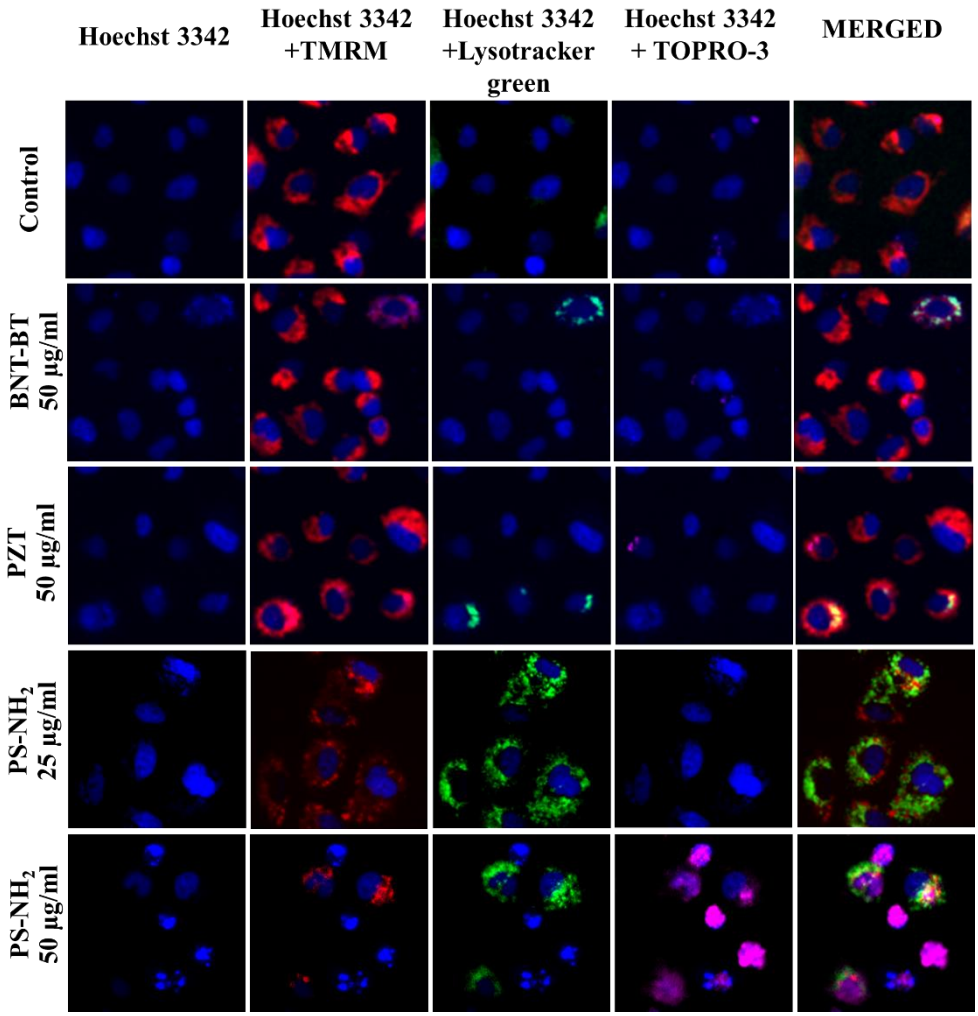

Figure 2. Representative images of A549 cells exposed to BNT-BT and PZT for 24 hours using Hoechst 33342, TMRM, Lysotracker® green, and TOPRO-3. A549 cells were exposed to increasing concentrations (6.25 to 100 µg/ml) of BNT-BT and PZT for 24, 48 and 72 h. The control was exposed to the represented by the medium without NPs (Control) and as a positive control for cytotoxicity cells were exposed to 25 and µg/ml PS-NH2 nanoparticles. Little alterations in cell physiology were observed after the exposure to BNT-BT and PZT nanoparticles, including hyperpolarization of the mitochondria and increased acidity of lysosomal compartments. Control cells did not show alterations of any of the parameters evaluated, as expected. Exposure to PS-NH_2 nanoparticles induced a decrease in the number of cells, mitochondrial membrane potential, plasma membrane integrity, increase in nuclear condensation and acidic compartments, as previously reported.

A combination of the nuclear parameters evaluated showed that there was no alteration in cell count and proliferation in A549 cells after the exposure to BNT-BT and PZT at any concentration or fixed time point tested up to 72h (Figure 3 cell intensity panel and Figure S2a). BNT-BT nanoparticles caused transient mitochondrial hyperpolarization that was observed after 24h of exposure at doses higher than 12.5 µg/ml, significant difference was found when compared with PZT nanoparticles and higher than 25 to 100 µg/ml when compared with the control cells ($p<0.05$). At the 48h time point the increment in mitochondrial membrane potential was significantly different to the effect of PZT nanoparticles at the concentration of 100 µg/ml ($p<0.05$), moreover, when compared with the control cells the difference was observed at the 50 and 100 µg/ml concentrations. This difference between the treatment with PZT and BNT-BT was not observed after 72h. However, the increase in TMRM fluorescence observed in cells exposed to BNT-BT nanoparticles, compared to control cells, was maintained at 100 µg/ml. In contrast, PZT nanoparticles did not alter the mitochondrial membrane potential at any of the times or concentrations tested (Figure 3 TMRM panel). The mitochondrial activity was also evaluated by measuring the bioreduction of a tetrazolium compound (3 - (4,5-dimethylthiazol-2-yl) - 5 - (3-carboxymethoxyphenyl) - 2 - (4-sulfophenyl)-2H-tetrazolium, inner salt) or MTS assay. The results (Figure S3b) showed increase in mitochondrial activity following BNT-BT nanoparticle exposure in agreement with the increased TMRM fluorescence observed by HCA. Mitochondria have a double function in cells: while in physiological conditions they are responsible to support cell bioenergetics through ATP production, mitochondria are also central to execution of apoptosis by releasing apoptogenic factors and promoting activation of the caspase cascade.[22] Hyperpolarization of the mitochondrial membrane is a transient event that precedes release of apoptogenic factors during apoptosis, mainly caused by ATP depletion, subsequent interruption of the proton pumps associated with the electron transport chain on the inner mitochondrial membrane and release of reactive oxygen species in the cytosol.[23, 24] Sustained hyperpolarization of the mitochondrial membrane was also reported in response to direct inhibition of the electron transport chain,[25], calcium disregulation[26, 27] or reactive oxygenspecies generation.[28, 29]

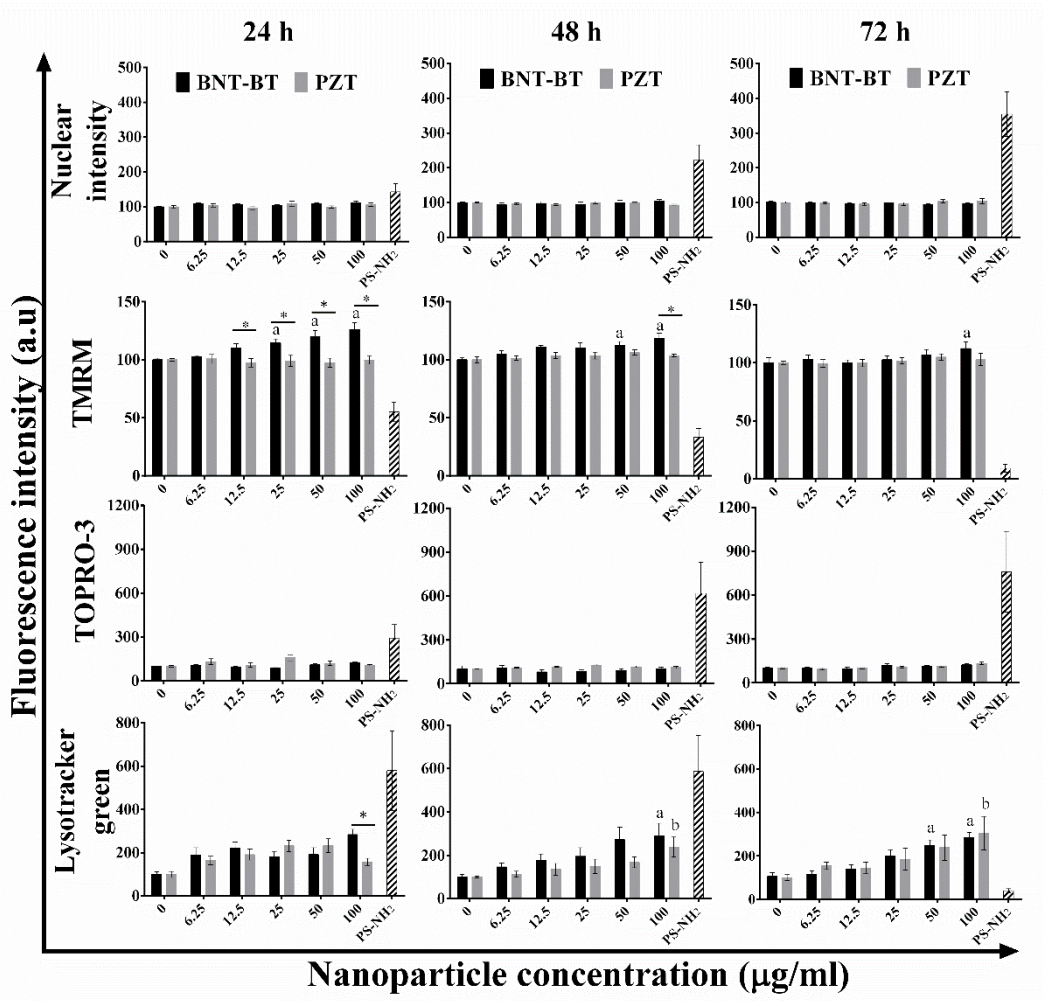

Figure 3. Effects of the exposure to BNT-BT and PZT nanoparticles in A549 cells. A549 cells were exposed to increasing concentrations of BNT-BT and PZT nanoparticles in dispersion (6.25 to 100 µg/ml) for 24, 48 and 72h. The nuclear intensity was evaluated by the fluorescent dye Hoechst 33342. Mitochondrial membrane potential, and plasma membrane permeability were measured by TMRM and TOPRO®-3, respectively. Acidic compartments were evaluated using Lysotracker® green dye. The data represent the mean ± SEM of three independent experiments. (a) Represents significant differences between the cells exposed to BNT-BT nanoparticles and control cells, (b) represents significant differences between the cells exposed to PZT nanoparticles and control cells and (*) represents the differences between BNT-BT and PZT with a $p<0.05$.

In our study we observed that exposure to high doses of BNT-BT NPs induced mitochondrial hyperpolarization, detected by increase in TMRM fluorescence intensity, which did not result in execution of apoptosis and was sustained over all the time points analysed, up to 72h. This phenomenon could be caused by many contributing factors, including potential generation of reactive oxygen species following exposure to BNT-BT NPs. Further, the sustained acidic pH of lysosomes, driven by ATP proton pumps on their membrane, may contribute to causing hyperpolarization of the mitochondrial membrane by sequestering ATP and H^+ from the electron transport chain in the mitochondria. Another parameter evaluated was plasma membrane integrity, the fluorescence intensity of the membrane impermeable DNA-binding fluorescent probe TOPRO®-3 remained unchanged after the exposure to BNT-BT or PZT nanoparticles at the concentrations and time points tested in this assay ($p>0.05$), indicating that exposure to the nanoparticles did not cause cell death or damage in cell membrane (Figure 3 TOPRO-3 panel). The levels of the intracytoplasmic enzyme lactate dehydrogenase (LDH) were measured in cell culture media in order to confirm TOPRO®-3 staining experiment outcome. LDH levels were comparable for cells exposed to nanoparticles and control cells (Figure S3b). BNT-BT nanoparticles did not induce acute toxicity at any of the concentrations tested, up to 100 µg/ml. To the best of our knowledge, there are no reports on the potential toxicity of BNT-BT or PZT nanoparticles. Moreover, very few studies have addressed the safety of other bismuth-based nanoparticles showing results that are in contrast to those shown here. Bare-bismuth (Bi) and bismuth ferrite (BiFe) nanoparticles caused low and acute toxicity by damaging the cell membrane in HELA and PC-12 cells after short-term exposure; however, the cells recovered after 48h.[30, 31] On the other hand, the oral exposure to bismuth citrate in complete animal models were found to be non-lethal, however, bismuth compounds accumulated exclusively in lysosomes of macrophages and parietal cells.[12] The fluorescent imaging analysis using Hoechst and TOPRO-3 to assess nuclear morphology and cell membrane integrity revealed that despite the toxicity of lead, PZT nanoparticles showed no changes in either parameter suggesting that cell viability was maintained after exposure. The lack of toxicity demonstrated by PZT nanoparticles was unexpected since other lead based nanoparticles such as lead sulfide (PbS) showed

antifungal activity[32] and decreased cell proliferation in algae *Dunaliella salina,*[33] furthermore, PbS can induce an inflammatory response in rat lung tissue.[34] The mechanism of lead-based nanoparticles-induced cell death is traditionally apoptotic, via oxidative stress resulting in a decrease in mitochondrial activity inducing apoptosome formation.[35] In the case of yeast cells, surface absorbed nanoparticles tend to damage the cell wall leading to the inhibition of cell proliferation and cell death and these responses are closely related with the nanoparticle size.[32]

Exposure to BNT-BT and PZT induces pH reduction of lysosomal compartments

Acidotropic dyes (Lysotracker® green) that stain lysosomes with acidic pH were used to assess alterations in lysosomal functionality. Significant increase in fluorescence intensity of Lysotracker® green was observed after exposure to 100 µg/ml of BNT-BT compared with PZT nanoparticles at 24h in the absence of cell death. The highest concentration of both PZT and BNT-BT nanoparticles showed significant increase in lysosome acidification at 48 and 72h when compared with control cells. However, no significant difference in lysosomal acidification was found between PZT and BNT-BT nanoparticles. At 72h, the concentration of 50 µg/ml of BNT-BT nanoparticles showed to be significantly different from the control cells. As nanoparticle concentration increased acidic compartments increased was also observed at all times tested (Figure 3 Lysotracker Green panel).

These data suggest that both nanoparticles affect the activity and functionality of lysosomes only at very high concentrations. Uptake of polymeric nanoparticles forming a biomolecular corona has been well characterized and includes uptake using clathrin-mediated, clathrin-independent endocytosis and intracellular trafficking through the endolysosomal pathway.[16]

Further polymeric nanoparticles that induce apoptosis caused reduction in lysosomal pH, followed by swelling and rupturing of the lysosomal membrane.[36] Dissolution may also happen once nanoparticles accumulate in vesicles with low pH such as lysosomes; nevertheless, dissolution efficacy depends on the time of residence and the enzymatic activity within these organelles.[37] In this study, BNT-BT nanoparticles showed less than two percent of bismuth dissolved in the extracellular media while PZT nanoparticles

showed less than seven percent of lead in solution. Taking into account that both bismuth and lead were the main components of BNT-BT and PZT respectively, this indicates that both nanoparticles were stable with low dissolution levels in standard cell culture conditions. The dissolution of nanoparticles can lead to the delivery of large amounts of toxic ions that can induce adverse biological responses in cells.[20] The toxic effects of ZnO,[19] and Bi[31] nanoparticles can be explained to a certain extent by the dissolution and release of active ions in the extracellular media. Therefore, we hypothesized that the lack of toxicity induced by both nanoparticles, in particular PZT, was due to the structure stability. After nanoparticles are taken up by cells their intracellular fate can determine the toxic impact on cells. The sustained increase in fluorescence intensity of Lysotacker green suggested that accumulation of BNT-BT and PZT nanoparticles in the lysosomes partially impaired lysosomal functionality. The effect, however, was only observed when cells were exposed to very high exposed doses of nanoparticles and did not result in the activation of cell death pathways, as previously described for PS-NH_2 nanoparticles.

BNT-BT and PZT nanoparticles accumulate mainly in lamellar bodies and lysosomes

In order to confirm the previous observations, Transmission Electron Microscopy, representative images are shown in Figure 4, assessed the subcellular localization of nanoparticles. The high electric conductivity of both BNT-BT and PZT nanoparticles allowed a clear contrast between the applied particles and biological structures. Nanoparticles were observed interacting with the cell membrane during the uptake process or inside subcellular organelles. Single or agglomerates of nanoparticles were localized mainly in lamellar bodies around the nucleus. Nanoparticles were also localized in lysosomes. The presence of nanoparticles in the lamellar bodies and lysosomes was consistent with the HCA data showed previously and with cellular uptake using the endolysosomal pathway. The localization of nanoparticles was independent of the time and type of nanoparticle. The cell morphology was normal as shown in the images of the complete cell and the enlarge images of the organelles (Figure S4). These data were confirmed by TEM images showing nanoparticles

interacting with the cellular membrane and accumulating in lamellar bodies or lysosome-like organelles. Lamellar bodies are multilayered vesicles with variable size between 0.1 to 2.4 µm, characterized by acidic pH environment and lysozyme activity[38] that specialize in the storage and secretion of surfactant proteins.

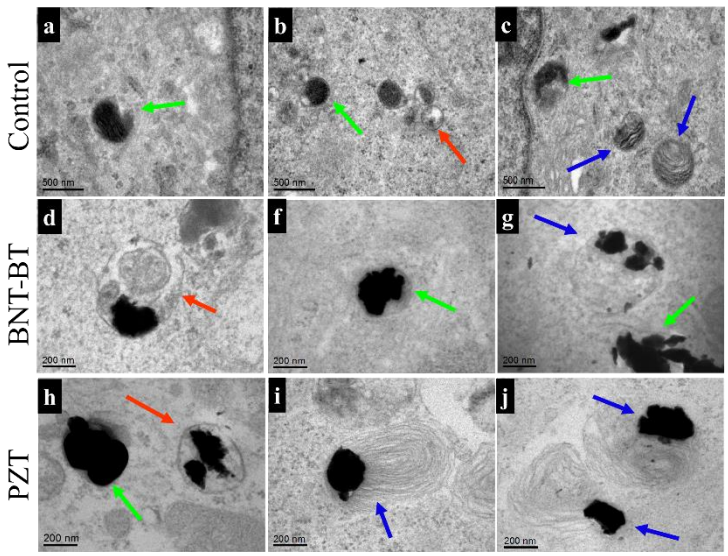

Figure 4. Subcellular localization of BNT-BT or PZT nanoparticles to lamellar bodies and lysosomes. Transmission electron microscopy (TEM) images of A549 cells exposed to 50 µg/ml of BNT-BT or PZT nanoparticles after 24, 48 and 72 hours of exposure. Representative images of (a-c) A549 cells without nanoparticles. Representative images of A549 cells exposed to 50 µg/ml of BNT-BT (d-g) or PZT (h-j) nanoparticles are shown. Blue arrows show lamellar bodies; Green arrows indicate lysosomes, and blue arrows show other vesicles related to endolysosomal pathway.

Lamellar bodies are connected with the endolysosomal system during internalization of nanoparticles in phagocytic and non-phagocytic cells. The induction of these vesicles in alveolar type II cells was suggested to be a defence mechanism for clearance of pathogen and foreign bodies.[39, 40] The exposure to particulate matter can induce morphological changes to alveolar cells, including formation of lamellar bodies; after 72h of constant exposure to diesel particulate matter, sub-micron particles can be observed in lamellar bodies.[41] The internalization of nanoparticles is directly related to their size[42] where small sizes are taken up faster when compared to micron size particles. In our study BNT-BT and PZT nanoparticles were observed by TEM inside

lamellar bodies even at the shortest time evaluated (24h). This suggests that both PZT and BNT-BT induce the production of lamellar bodies and probably surfactant proteins faster than sub-micron particles[41] and is likely related to the size of the nanoparticles.

BNT-BT and PZT nanoparticle uptake by A549 cell in a time dependent manner

Atomic spectrometry was performed to quantify nanoparticles taken up by cells at different exposure times. The apparent decrease in the relative uptake percentage was observed at increasing concentrations of nanoparticles at all times (except for PZT for 1h), this apparent decrease could be related with to potential agglomeration of the nanoparticles at higher concentrations that decrease the nanoparticles available for cell uptake. However, these differences were not significant. (Figure 5 a and b).

After 1h of nanoparticle exposure A549 cells internalized 10% of the dose of both tested nanoparticles; this phenomenon was independent of the type of nanoparticle. Overall the percentage of nanoparticles inside cells increased with time and reached 50% after 48h of continuous nanoparticle exposure prior normalization per 10^6 cells. The presence of nanoparticles inside cells was dependent of the time. In order to evaluate the uptake progression at different incubation times the data was normalize against time (1, 6, 24 and 48h) (Figure 5 c, d, c' and d'). A linear relationship was observed at 1h (r^2=0.987); 6h (r^2=0.960); 24h (r^2=0.999); and 48h (r^2=0.978) for BNT-BT. Also, for PZT high r^2 values were observed at each time point 1h (r^2=0.963); 6h (r^2=0.989); 24h (r^2=0.894); and 48h (r^2=0.994). The slopes were compared indicating that the velocity of nanoparticle uptake was significantly faster at the first hour of exposure than at any other time tested ($p<0.05$); no significant difference was found among 6, 24, and 48h uptake velocity. Both particles showed similar uptake behavior (Figure 5 c and d) and reached the stationary phase after 6h of exposure (Figure S5). Our study of nanoparticle uptake using atomic spectrometry delivered results that are consistent with previous studies of uptake of fluorescently-labelled nanoparticles performed by flow cytometry,[43] suggesting that atomic spectrometry can be used as a reliable method to monitor uptake of nanoparticles alternatively to flow cytometry. Next we analyzed the uptake rates of the nanoparticles in our cell model. The uptake of BNT-BT and PZT nanoparticles was dependent on the concentration of nanoparticles in the medium and the incubation time,

showing a first order kinetics trend. We were able to quantify nanoparticles after one hour of exposure.

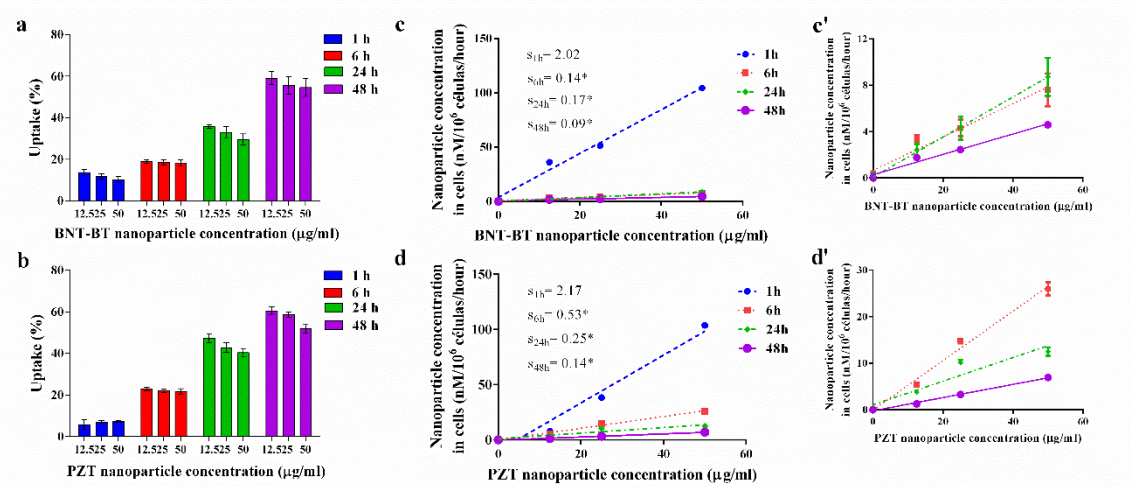

Figure 5. Time-resolved uptake of BNT-BT and PZT by A549 cells. Cells were incubated with increasing concentrations of BNT-BT (a, c, c') and PZT (b, d, d') nanoparticles. The metal content of bismuth and lead was measured by atomic spectrometry and the concentration of nanoparticles was calculated according to the percentage of metal in each nanoparticle. (a) and (b) show the percentage of cellular uptake compared with the cell culture media. (c) and (d) indicate the concentration of nanoparticles normalized by number of cells and hour. (c') and (d') represent a magnification of (c) and (d) at 6, 24 and 48h uptake. The graphs show the mean of three independent experiments ± SEM performed in triplicate, (s) indicates the slope at each time point.

However, the composition of the nanoparticles seemed to have no influence on the uptake rates as both PZT and BNT-BT showed similar uptake trends. Other authors have shown that characteristics such as particle number and total surface area are not a primary factor during the uptake.[44] Size is considered the most important characteristic affecting nanoparticle uptake; due to the assembly patterns of receptor clusters on the plasma membrane of cells and cell membrane thermodynamic forces 50 nm for BNT-BT and PZT suggest that cells started internalizing nanoparticles already during the first hour and reached the stationary phase (saturation capacity) after 6h of exposure. This

was in agreement with other uptake studies for metallic nanoparticles,[45-47] moreover, decrease in uptake velocity over time could be a result of dilution of the nanoparticle concentration inside the cells due to cell division.[48]

Conclusions

In this study, PZT and a potential replacement candidate BNT-BT were characterized and dispersed in order to compare their physicochemical characteristics and potential cytotoxicity. Our data demonstrate that both BNT-BT and PZT nanoparticles exhibited a non-harmful behavior in A549 cells, as demonstrated by the absence of changes in cell morphology, and cell membrane integrity. The nanoparticles showed similar uptake behavior, following a first order kinetic during the 48h exposure and were localized inside the cells in lamellar bodies and other lysosome-like organelles probably for neutralizing or excretion of the nanoparticles. Regardless the presence of nanoparticles in acidic organelles no toxicity was observed probably due to the high stability of the perovskite structure after the synthesis. Overall these effects were observed only at very high exposed doses of nanoparticles, suggesting high biocompatibility for both BNT-BT and PZT nanoparticles. However, despite the nontoxic effects of PZT nanoparticles these still contains a powerful toxic compound, i.e. lead oxide, which could be released in the environment or workplace during manufacturing process of piezoelectrics. Taking this in account, we found that higher quantities of lead ions were released into the cellular environment during a 24h incubation period. The slow release of these toxic ions did not affect cell viability at the time points or concentrations tested; however, this result suggests that PZT nanoparticles over time, can create an environmental hazard. Finally, we show that BNT-BT nanoparticles are an ideal non-toxic replacement for lead-based nanoparticles due to their stability, similar physico-chemical properties and high biocompatibility of the engineered nanoparticles, they present a more suitable less hazardous option during manufacturing and in occupational health. This approach may lead to important developments in the regulatory approval of new bismuth compounds for the lead replacement in a wide range of applications in the industry including nanomedicine and green energy generation.

Experimental

Chemicals

All reagents for cell culture and phosphate-buffered saline solution (PBS) were purchased from Gibco (Life technologies). Fluorescent probes Hoechst 33342, tetramethyl rhodamine methyl ester perchlorate (TMRM), LysoTracker® green, and TOPRO®-3 were purchased from Life Technologies. Nitric acid (HNO_3), perchloric acid ($HClO_4$), hydrogen chloride (HCl), and sodium hydroxide (NaOH) were purchased from Merck. Bovine serum albumin (BSA), sodium tetrahydroborate ($NaBH_4$) and glutaraldehyde were bought from Sigma-Aldrich.

Preparation and physicochemical characterization of nanoparticles

BNT-BT and PZT nanoparticles were synthesized at CINVESTAV-Queretaro following the powder mixtures and solid state reaction methodology and provided in a dry powder form. Briefly, the nanoparticles were suspended in phosphate buffer pH 7.4 at a concentration of 10 mg/ml, and then the mixture was probe sonicated for 15 minutes at 20 W in order to improve mixing. BSA was added at a concentration of 1 mg per mg of nanoparticles to aid the dispersion stability. As the dispersions generated contained micrometric size aggregates centrifugation steps (200 x g for 20 minutes) were applied to isolate particles in the nanoscale.

Size distribution of the dispersions were determined in PBS by both dynamic light scattering (DLS) with a Zetasizer Nano-ZS (Malvern Instruments LTD) and differential centrifugal sedimentation (DCS) with a CPS Disc Centrifuge (DC24000)[49] at a concentration of 50 µg/ml of nanoparticles in solution. Size distribution was also assessed complete cell culture medium, i.e. Dulbecco's Modified Eagle Medium (DMEM) supplemented with 10% fetal bovine serum. PBS supplemented with 10 mg/ml BSA and cell culture medium without particles were used as a control to exclude potential protein aggregates in the solvents.[50] The zeta potential was determined by Laser Doppler Anemometer with a Zetasizer Nano-ZS (Malvern Instruments LTD).

A drop of the nanoparticles in dispersion was placed onto a silicon support and analyzed by scanning electron microscopy (SEM). This analysis was carried out with an AURIGA field emission SEM (Carl Zeiss).

Cell Lines

Human bronchoalveolar carcinoma A549 cells obtained from American Type Culture Collection (ATCC) were grown in DMEM supplemented with 10% fetal bovine serum, 50 Units/ml of penicillin G and 50 µg/ml of streptomycin sulphate called complete medium (cDMEM). The cultures were maintained in a humidified incubator at 37°C and 5% CO_2. Cells were passaged every three days.

High Content Analysis

High Content Analysis was performed according to Anguissola *et al*. (2014). Briefly, $1x10^4$ cells were seeded in 96-well plates and grown for 24h. BNT-BT or PZT nanoparticle dispersions, prepared as described above, were added to the cells to a final concentration of 0, 6.25, 12.5, 25, 50 and 100 µg/ml in cell culture media. Cells and nanoparticles were incubated for 24, 48, and 72h. After each time exposure a mixture of fluorescent probes (400 nM Hoechst 33342, 20 nM TMRM, 200 nM of LysoTracker® green and 800 nM of TOPRO®-3) was added to the cells for 1h at 37°C in a CO_2 incubator. Cells were analyzed by High Content Analysis with the Arrayscan VTI 740 (Thermo Scientific). The fluorescence intensity was collected using a combination of excitation/emission filters[18] and analysis was performed using Thermo Scientific proprietary software. 50 nm Amine-modified PS-NH_2 nanoparticles at the concentration of 25 and 50 µg/ml were used as a positive control for apoptosis induced by nanoparticles.[18]

Transmission Electron Microscopy

Transmission electron microscopy (TEM) was used to assess the subcellular localization of nanoparticles in A549 cells. A549 cells were treated with 50 µg/ml of BNT-BT or PZT nanoparticles for 24, 48, and 72h. The cells were processed according to standard procedures.[51] Briefly cells were fixed at room temperature in 2.5% glutaraldehyde (pH

7.3). Osmium tetroxide (1%) was used as a postfix treatment. The dehydration steps were performed with increasing concentrations of ethanol. The samples were immersed in an ethanol/Epon (1:1 v/v) mixture for 1h, before the samples were transferred to pure Epon and embedded at 37° C for 2h. Final polymerization was accomplished at 60 °C for 24h. Ultrathin sections of 80 nm were obtained with a diamond knife using a Leica U6 ultramicrotome. The sections were mounted on copper grids and were stained with uranyl acetate and lead citrate. The microscope JEOL 1400 (JEOL Ltd) was operated at an accelerating voltage of 80 kV in order to analyze the samples.

Cell exposure to nanoparticles and acid digestion

Atomic absorption spectrometry and atomic fluorescence spectrometry were performed in order to investigate uptake kinetics of lead-based and Bismuth-based nanoparticles respectively. Briefly, A549 cells (1.5 x 10^5 cells/well) were seeded in 6-well plates and incubated for 24h at 37°C. Three concentrations (6.25, 12.5 and 25 µg/ml) of the BNT-BT or PZT nanoparticles were exposed to the cells for 1, 6, 24, and 48h. An aliquot of each treatment was centrifuged (after 1h at 37ºC) at 20000 g during 1h and the supernatant was recover as well as the nanoparticles in the pellet. After exposure cells were washed three times with PBS. The cell culture medium and the PBS from the washes were collected in the same tube. The cells were trypsinized, harvested and transferred to another tube. Subsequently, the cells were counted by trypan blue exclusion using the TC10™ automated cell counter (Bio-Rad). The medium and the cells were subjected to a two stage acid digestion. For the first stage, HNO_3 and $HClO_4$ were added in a proportion 5:1, at 100° C for 1h. For the second stage, 3 ml of HNO_3 were added and the temperature was increased to 160 °C in order to concentrate the sample to 1 ml.[52] Samples were suspended in 3 ml of concentrated HCl and 6 ml of ultrapure water (Millipore) to determine bismuth content or 9 ml of ultrapure water (Millipore) to determine lead content.

Bismuth detection by atomic fluorescence spectrometry

A continuous-flow hydride generation atomic fluorescence spectrometer Excalibur (PS Analytical) equipped with hollow cathode lamp for bismuth (Photron) was employed

for the detection of bismuth. The gaseous hydride was formed after mixing the sample with 0.7 % m/v of $NaBH_4$ in 0.1 M of NaOH.[53] The calibration graph was prepared with at least 6 points between 0 and 196 ppb. Two internal standards of 5 and 50 ppb and the 1643e NIST standard were used in order to evaluate the quality of the determination.

Lead detection by atomic absorption spectrometry

Lead was quantified using an AAnalyst 100 flame atomic absorption spectrometer (Perkin Elmer), equipped with a lead hollow cathode lamp and air-acetylene burner. The wavelength used was 283.3 nm, the lamp current was 10 mA, and the band pass was 0.70 nm for lead detection.[54] A calibration curve was prepared with at least 6 concentrations between 0 and 10 ppm. An internal standard of 5 ppm was used in order to evaluate the quality control of the data.

Calculation of uptake rates

Uptake of nanoparticles was calculated taking into account the percentage of bismuth or lead in the particle and the molar mass of BNT-BT and PZT. The data were normalized by 10^6 cells and by hour. The velocity of nanoparticle uptake at different time points was calculated by fitting the normalized data with a linear regression model.

Data analysis and statistics

The High Content Analysis results were normalized against the control cells under the same conditions. Comparisons against the control were performed using one-way ANOVA and Dunnett's *post-hoc* tests. Groups were compared by two-way ANOVA followed by Bonferronis *post-hoc*-tests. P values of $p<0.05$ indicated significant differences among samples.

For the uptake analysis the slopes were compared among each other. P values of $p<0.05$ were considered significantly different. The software Graph Pad Prism V.5 (Graph Pad Software) was used to perform the data analysis.

Acknowledgements

This work was funded by EU FP7 EU-Mexico Collaborative project BisNano (NMP4-EU-Mexico-2013-263878). Research activities were supported by CONACyT and the European Science Foundation Research Networking Programme EpitopeMap. The authors gratefully acknowledge Marisela Uribe-Ramirez, Angel Barrera-Hernández and Luz del Carmen Sanchez-Peña for technical support and QFB Sirenia Gonzales from the Electron Microscopy Unit in CINVESTAV.

Notes

[a] Departamento de Toxicología. Centro de Investigación y de Estudios Avanzados del IPN (CINVESTAV-IPN), Av. Instituto Politecnico Nacional No. 2508, Col. San Pedro Zacatenco, 07360, Mexico Distrito Federal, Mexico.

[b] Centre for Bionano Interactions, School of Chemistry and Chemical Biology, University College Dublin, Belfield, Dublin 4, Ireland

[c] Unidad Quéretaro. Centro de Investigación y de Estudios Avanzados del IPN (CINVESTAV-IPN), Libramiento Norponiente No. 2000, Frac. Real de Juriquilla, Queretaro, 76230 Mexico.

* Corresponding authors e-mails: avizcaya@cinvestav.mx and ldelrazo@cinvestav.mx

Electronic Supplementary Information (ESI) available. See DOI: 10.1039/b000000x/

References

1. E. J. Cho, H. Holback, K. C. Liu, S. A. Abouelmagd, J. Park and Y. Yeo, *Molecular pharmaceutics*, 2013, 10, 2093-2110.
2. G. Oberdorster, E. Oberdorster and J. Oberdorster, *Environmental health perspectives*, 2005, 113, 823-839.
3. N. Nuraje and K. Su, *Nanoscale*, 2013, 5, 8752-8780.
4. P. K. Panda, *J Mater Sci*, 2009, 44, 5049-5062.
5. R. Dittmer, W. Jo, J. Rodel, S. Kalinin and N. Balke, *Adv Funct Mater*, 2012, 22, 4208-4215.

6. W. F. Liu and X. B. Ren, *Physical review letters*, 2009, 103.
7. B. Parija, T. Badapanda, S. Panigrahi and T. P. Sinha, *J Mater Sci-Mater El*, 2013, 24, 402-410.
8. N. C. Papanikolaou, E. G. Hatzidaki, S. Belivanis, G. N. Tzanakakis and A. M. Tsatsakis, *Medical science monitor : international medical journal of experimental and clinical research*, 2005, 11, RA329-336.
9. M.-S. Yoon, N. H. Khansur, B.-K. Choi, Y.-G. Lee and S.-C. Ur, *Ceram Int*, 2009, 35, 3027-3036.
10. S. Trujillo, J. Kreisel, Q. Jiang, J. H. Smith, P. A. Thomas, P. Bouvier and F. Weiss, *Journal of Physics: Condensed Matter*, 2005, 17, 6587.
11. J. C. Delchier, P. Malfertheiner and R. Thieroff-Ekerdt, *Aliment Pharm Ther*, 2014, 40, 171-177.
12. A. Larsen, M. Martiny, M. Stoltenberg, G. Danscher and J. Rungby, *Pharmacol Toxicol*, 2003, 93, 82-90.
13. C. Som, M. Berges, Q. Chaudhry, M. Dusinska, T. F. Fernandes, S. I. Olsen and B. Nowack, *Toxicology*, 2010, 269, 160-169.
14. A. E. Nel, L. Madler, D. Velegol, T. Xia, E. M. Hoek, P. Somasundaran, F. Klaessig, V. Castranova and M. Thompson, *Nature materials*, 2009, 8, 543-557.
15. A. Nel, T. Xia, L. Madler and N. Li, *Science*, 2006, 311, 622-627.
16. K. Shapero, F. Fenaroli, I. Lynch, D. C. Cottell, A. Salvati and K. A. Dawson, *Molecular bioSystems*, 2011, 7, 371-378.
17. J. Dausend, A. Musyanovych, M. Dass, P. Walther, H. Schrezenmeier, K. Landfester and V. Mailander, *Macromolecular bioscience*, 2008, 8, 1135-1143.
18. S. Anguissola, D. Garry, A. Salvati, P. J. O'Brien and K. A. Dawson, *PloS one*, 2014, 9, e108025.
19. T. Xia, M. Kovochich, M. Liong, L. Madler, B. Gilbert, H. Shi, J. I. Yeh, J. I. Zink and A. E. Nel, *ACS nano*, 2008, 2, 2121-2134.
20. S. Sabella, R. P. Carney, V. Brunetti, M. A. Malvindi, N. Al-Juffali, G. Vecchio, S. M. Janes, O. M. Bakr, R. Cingolani, F. Stellacci and P. P. Pompa, *Nanoscale*, 2014, 6, 7052-7061.
21. P. J. O'Brien, *Basic Clin Pharmacol Toxicol*, 2014, 115, 4-17.
22. S. W. Tait and D. R. Green, *Nature reviews. Molecular cell biology*, 2010, 11, 621-632.
23. J. A. Sanchez-Alcazar, J. G. Ault, A. Khodjakov and E. Schneider, *Cell death and differentiation*, 2000, 7, 1090-1100.
24. D. B. Zorov, M. Juhaszova and S. J. Sollott, *Biochimica et biophysica acta*, 2006, 1757, 509-517.
25. M. Forkink, G. R. Manjeri, D. C. Liemburg-Apers, E. Nibbeling, M. Blanchard, A. Wojtala, J. A. Smeitink, M. R. Wieckowski, P. H. Willems and W. J. Koopman, *Biochimica et biophysica acta*, 2014, 1837, 1247-1256.
26. D. Poburko, J. Santo-Domingo and N. Demaurex, *The Journal of biological chemistry*, 2011, 286, 11672-11684.
27. J. Cao, Y. Liu, L. Jia, H. M. Zhou, Y. Kong, G. Yang, L. P. Jiang, Q. J. Li and L. F. Zhong, *Free radical biology & medicine*, 2007, 43, 968-975.
28. M. J. Liu, P. Y. Yue, Z. Wang and R. N. Wong, *Cancer letters*, 2005, 224, 229-241.

29. P. Gergely, Jr., B. Niland, N. Gonchoroff, R. Pullmann, Jr., P. E. Phillips and A. Perl, *Journal of immunology*, 2002, 169, 1092-1101.
30. Q. Song, Y. P. Liu, Z. Y. Jiang, M. L. Tang, N. Li, F. F. Wei and G. S. Cheng, *Journal of Nanoparticle Research*, 2014, 16.
31. Y. Luo, C. Wang, Y. Qiao, M. Hossain, L. Ma and M. Su, *Journal of materials science. Materials in medicine*, 2012, 23, 2563-2573.
32. M. Sun, Q. Yu, M. Hu, Z. Hao, C. Zhang and M. Li, *Journal of hazardous materials*, 2014, 273, 7-16.
33. H. Zamani, A. Moradshahi, H. D. Jahromi and M. H. Sheikhi, *Aquatic toxicology*, 2014, 154, 176-183.
34. Q. Li, X. Hu, Y. Bai, M. Alattar, D. Ma, Y. Cao, Y. Hao, L. Wang and C. Jiang, *Food and chemical toxicology : an international journal published for the British Industrial Biological Research Association*, 2013, 60, 213-217.
35. Q. Jia, X. Ha, Z. Yang, L. Hui and X. Yang, *Toxicology mechanisms and methods*, 2012, 22, 705-710.
36. F. Wang, M. G. Bexiga, S. Anguissola, P. Boya, J. C. Simpson, A. Salvati and K. A. Dawson, *Nanoscale*, 2013, 5, 10868-10876.
37. L. A. Schaider, D. B. Senn, D. J. Brabander, K. D. McCarthy and J. P. Shine, *Environmental science & technology*, 2007, 41, 4164-4171.
38. G. Schmitz and G. Muller, *Journal of lipid research*, 1991, 32, 1539-1570.
39. M. Davoren, E. Herzog, A. Casey, B. Cottineau, G. Chambers, H. J. Byrne and F. M. Lyng, *Toxicology in vitro : an international journal published in association with BIBRA*, 2007, 21, 438-448.
40. J. R. Wright and L. G. Dobbs, *Annual review of physiology*, 1991, 53, 395-414.
41. V. Esposito, A. Lucariello, L. Savarese, M. P. Cinelli, F. Ferraraccio, A. Bianco, A. De Luca and G. Mazzarella, *Environmental pollution*, 2012, 171, 162-167.
42. T. dos Santos, J. Varela, I. Lynch, A. Salvati and K. A. Dawson, *Small*, 2011, 7, 3341-3349.
43. A. Salvati, C. Aberg, T. dos Santos, J. Varela, P. Pinto, I. Lynch and K. A. Dawson, *Nanomedicine : nanotechnology, biology, and medicine*, 2011, 7, 818-826.
44. L. K. Limbach, Y. Li, R. N. Grass, T. J. Brunner, M. A. Hintermann, M. Muller, D. Gunther and W. J. Stark, *Environmental science & technology*, 2005, 39, 9370-9376.
45. J. Davda and V. Labhasetwar, *International journal of pharmaceutics*, 2002, 233, 51-59.
46. B. D. Chithrani, A. A. Ghazani and W. C. Chan, *Nano letters*, 2006, 6, 662-668.
47. A. Lesniak, A. Salvati, M. J. Santos-Martinez, M. W. Radomski, K. A. Dawson and C. Aberg, *Journal of the American Chemical Society*, 2013, 135, 1438-1444.
48. J. A. Kim, C. Aberg, A. Salvati and K. A. Dawson, *Nature nanotechnology*, 2012, 7, 62-68.
49. A. S. Pitek, D. O'Connell, E. Mahon, M. P. Monopoli, F. Baldelli Bombelli and K. A. Dawson, *PloS one*, 2012, 7, e40685.
50. R. C. Murdock, L. Braydich-Stolle, A. M. Schrand, J. J. Schlager and S. M. Hussain, *Toxicological Sciences*, 2008, 101, 239-253.

51. D. Ye, K. A. Dawson and I. Lynch, *The Analyst*, 2014, DOI: 10.1039/c4an01276c.
52. D. H. Cox, *Journal of analytical toxicology*, 1980, 4, 207-211.
53. P. Cava-Montesinos, M. L. Cervera, A. Pastor and M. de la Guardia, *Journal of AOAC International*, 2003, 86, 815-822.
54. NIOHS, *NIOSH Manual of Analytical Methods (NMAM) Method 7082: Lead by flame AAS.*, Department of Health and Human Services, Centers for Disease Control and Prevention, National Institute for Occupational Safety and Health, DHHS (NIOSH), 1994